Dynamics of atom-mediated photon-photon scattering

M. W. Mitchell, Cindy I. Hancox, and R. Y. Chiao
Department of Physics, University of California at Berkeley, Berkeley, California 94720
(Received 18 February 2000; revised manuscript received 12 June 2000; published 19 September 2000)

The mediated photon-photon interaction due to the resonant Kerr nonlinearity in an inhomogeneously broadened atomic vapor is considered. The time scale for photon-photon scattering is found to be determined by the inhomogeneous broadening and the magnitude of the momentum transfer. This time can be shorter than the atomic relaxation time. Effects of atom statistics are included and the special case of small-angle scattering is considered. In the latter case, the time scale of the nonlinear response remains fast, even though the linear response slows as the inverse of the momentum transfer. Measurements of temporal and angular correlations show good agreement with theory.

PACS number(s): 42.50.Ct, 42.65.Hw

I. INTRODUCTION

Recently there has been experimental and theoretical interest in the nonlinear optics of confined light [1]. A medium possessing an optical Kerr nonlinearity and confined within a planar or cylindrical Fabry-Perot resonator gives rise to new nonlinear optical phenomena such as soliton filtering and bilateral symmetry breaking [2,3]. The classical nonlinear optics of this system is described by the complex Ginzburg-Landau equation (CGLE),

$$\frac{\partial E}{\partial t}=\frac{ic}{2n_0k}\nabla_\perp^2 E+i\omega A\frac{n_2}{n_0}|E|^2E+\frac{ic\Delta k}{n_0}E-\Gamma(E-E_d), \tag{1}$$

where E is the electric field envelope, k is the longitudinal wave number, $\omega=ck/n_0$ is the field envelope angular frequency, A is a mode overlap factor, Δk is the wave-number mismatch from the linear-cavity response, and Γ is the field-amplitude decay rate. The classical dynamics of Eq. (1) describes the mean-field behavior of a system of interacting photons coherently coupled to an external reservoir. A photonic system of this sort is a versatile model system for condensed-matter physics in reduced dimensions [4], as the parameters Δk, n_2, Γ, and E_d in Eq. (1) are subject to experimental control. In particular, an atomic vapor can provide a strong Kerr nonlinearity which is tunable both in strength and in sign. In this case the nonlinearity arises from the saturation of the linear refractive index, which is a strong function of the drive laser frequency near an absorption resonance.

Some of the most interesting proposed experiments for this system, including generation of few-photon bound states [5], direct observation of the Kosterlitz-Thouless transition in an optical system [4], and observation of quantum corrections to the elementary excitation spectrum of a one-dimensional (1D) photon gas [6,7], intrinsically involve photon correlations. For this reason, it is important to understand the microscopic (and not just mean-field) behavior of photons in an optical Kerr medium. We specifically consider saturation of the resonant electronic polarization of a Doppler-broadened atomic vapor, a medium which has been proposed for quantum cavity nonlinear optics experiments and used to observe a nonlinear cavity mode [2]. Thus the system under consideration involves dispersion, loss, inhomogeneous broadening, and the continuum of transverse modes in an extended resonator.

Sophisticated techniques have been developed for treating mediated interactions among photons in nonlinear media. One approach is to obtain an effective theory in which the quanta are excitations of coupled radiation-matter modes, by canonical quantization of the macroscopic field equations [8,9], or by direct attack on a microscopic Hamiltonian [10]. This approach has the advantage of generality and is suited to multimode problems, but has basic difficulties with loss and dispersion near resonance [11–13]. Microscopic treatments include Scully-Lamb-type theory [14,15] and application of phase-space methods [16,17]. A strength of these techniques is their ability to handle relaxation and population changes. They are, however, cumbersome to apply to inhomogeneously broadened media and to multimode problems.

In this paper we characterize the atom-mediated photon-photon interaction using an accurate microscopic model and perturbation calculations. This allows us to determine the time scale of the mediated photon-photon interaction in the atomic vapor, despite the complexity of the medium. We find that the interaction is fast and not intrinsically lossy, even for small momentum transfer. Thus the medium is suitable for quantum optical experiments, including experiments using the nonlinear Fabry–Perot resonator as a model for the interacting Bose gas.

II. SCATTERING CALCULATIONS

The complete system is treated as the quantized electromagnetic field interacting via the dipole interaction with a vapor of atoms of mass M. The perturbation calculations are performed in momentum space, as is natural for thermodynamic description of the atomic vapor. This also makes simple the inclusion of atomic recoil effects. The dipole interaction term is identified as the perturbation, so that the eigenstates of the unperturbed Hamiltonian are direct products of Fock states for each field. In the rotating-wave approximation, the unperturbed and perturbation Hamiltonians are

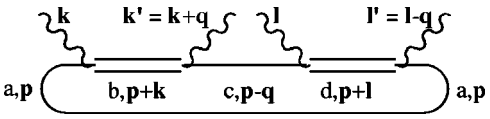

FIG. 1. Photon-photon scattering at a single atom.

$$H_0=\sum_{\mathbf{k},\alpha}\hbar ck a^\dagger_{\mathbf{k},\alpha}a_{\mathbf{k},\alpha}+\sum_{n,\mathbf{p}}\left(\hbar\omega_n+\frac{\hbar^2\mathbf{p}^2}{2M}\right)c^\dagger_{n,\mathbf{p}}c_{n,\mathbf{p}}, \quad (2)$$

$$H'=-\mathbf{E}(\mathbf{x})\cdot\mathbf{d}(\mathbf{x})$$
$$=-\sum_{\mathbf{k},\alpha}\sqrt{\frac{2\pi\hbar ck}{V}}\sum_{n,m,\mathbf{p}} i\mathbf{e}_{\mathbf{k},\alpha}\cdot\boldsymbol{\mu}_{nm}c^\dagger_{n,\mathbf{p}+\mathbf{k}}c_{m,\mathbf{p}}a_{\mathbf{k},\alpha}+\text{H.c.}, \quad (3)$$

where $a_{\mathbf{k},\alpha}$ is the annihilation operator for a photon of momentum $\hbar\mathbf{k}$ and polarization α, $c_{n,\mathbf{p}}$ is the annihilation operator for an atom in internal state n with center-of-mass momentum $\hbar\mathbf{p}$, $\mathbf{E}$ is the quantized electric field, and $\mathbf{d}$ is the atomic dipole field. Polarization plays only a very minor role in this discussion so polarization indices will be omitted from this point forward.

The simplest mediated interaction is photon-photon scattering, which transfers momentum from one photon to another by temporarily depositing this momentum in the medium. Specifically, photons with momenta $\mathbf{k},\mathbf{l}$ are consumed and photons with momenta $\mathbf{k}'\equiv\mathbf{k}+\mathbf{q},\mathbf{l}'\equiv\mathbf{l}-\mathbf{q}$ are produced. The lowest-order processes to do this are fourth order, so we look for relevant terms in H'^4. A parametric process, i.e., one which leaves the medium unchanged, sums coherently over all atoms which could be involved [18]. Due to this coherence, the rates of parametric processes scale as the square of N/V, the number density of atoms. In contrast, incoherent loss processes such as Rayleigh and Raman scattering scale as N/V. Thus for large atomic densities, a given photon is more likely to interact with another photon than it is to be lost from the system.

In this sense, the interaction is not intrinsically lossy, as are some optical Kerr nonlinearities such as optical pumping or thermal blooming. The latter processes require absorption of photons before there is any effect on other photons. For this reason, they are unsuitable for quantum optical experiments such as creation of a two-photon bound state.

One parametric process, photon-photon scattering at a single atom, is described by the diagram of Fig. 1. The relevant terms in H'^4 contain

$$c^\dagger_{a,\mathbf{p}}c_{d,\mathbf{p}+\mathbf{l}'}a^\dagger_{\mathbf{l}'}c^\dagger_{d,\mathbf{p}+\mathbf{l}'}c_{c,\mathbf{p}-\mathbf{q}}a_{\mathbf{l}}c^\dagger_{c,\mathbf{p}-\mathbf{q}}c_{b,\mathbf{p}+\mathbf{k}}a^\dagger_{\mathbf{k}'}c^\dagger_{b,\mathbf{p}+\mathbf{k}}c_{a,\mathbf{p}}a_{\mathbf{k}} \quad (4)$$

or permutations $\mathbf{k}'\leftrightarrow\mathbf{l}'$, $\mathbf{k}\leftrightarrow\mathbf{l}$ for a total of four terms. Here $\mathbf{p}$ is the initial atomic momentum and a through d index the atomic states involved. With the assumption that no atoms are initially found in the upper states b and d, i.e., $n_b=n_d=0$, this reduces to

$$n_{a,\mathbf{p}}(1\pm n_{c,\mathbf{p}-\mathbf{q}})a^\dagger_{\mathbf{l}'}a_{\mathbf{l}}a^\dagger_{\mathbf{k}'}a_{\mathbf{k}}, \quad (5)$$

where the n are number operators for the atomic modes and the upper and lower signs hold for Bose and Fermi gases, respectively. The difference for atoms of different statistics reflects the fact that the scattering process takes the atom through an intermediate momentum state which could be occupied. Occupation of this intermediate state enhances the process for Bose gases but suppresses it for Fermi gases.

A thermal average of the relevant terms in H'^4 gives the thermally averaged effective perturbation

$$\langle H'_{\text{eff}}\rangle=\frac{(2\pi)^3}{V}\sum_{\mathbf{klk}'\mathbf{l}'}V_{\mathbf{l}'\mathbf{k}'\mathbf{lk}}a^\dagger_{\mathbf{l}'}a_{\mathbf{l}}a^\dagger_{\mathbf{k}'}a_{\mathbf{k}}, \quad (6)$$

where

$$V_{\mathbf{l}'\mathbf{k}'\mathbf{lk}}\equiv\sum_a\int d^3\mathbf{p}\, v_{\text{eff}}(\mathbf{p},a,c)\langle n_{a,\mathbf{p}}\rangle\sum_c(1\pm\langle n_{c,\mathbf{p}-\mathbf{q}}\rangle), \quad (7)$$

$$v_{\text{eff}}(\mathbf{p},a,c)=v^{(1)}_{\text{eff}}+v^{(2)}_{\text{eff}}+v^{(3)}_{\text{eff}}+v^{(4)}_{\text{eff}}, \quad (8)$$

$$v^{(1)}_{\text{eff}}=\frac{c^2\sqrt{klk'l'}}{(2\pi)^4\hbar}\sum_{bd}(\mathbf{e}_{\mathbf{l}'}\cdot\boldsymbol{\mu}_{da})^*\mathbf{e}_{\mathbf{l}}\cdot\boldsymbol{\mu}_{dc}(\mathbf{e}_{\mathbf{k}'}\cdot\boldsymbol{\mu}_{bc})^*\mathbf{e}_{\mathbf{k}}\cdot\boldsymbol{\mu}_{ba}$$
$$\times[R^{(1)}_1R^{(1)}_2R^{(1)}_3]^{-1}, \quad (9)$$

and similar expressions are obtained for $v^{(2-4)}_{\text{eff}}$. $\langle n_{a,\mathbf{p}}\rangle$ is the average occupancy of the atomic state $|a,\mathbf{p}\rangle$. The $R^{(1)}_i$ are the resonance denominators

$$R^{(1)}_1=c(k+l-k')-\frac{\hbar}{M}[\mathbf{p}\cdot\mathbf{l}'+l'^2/2]-\omega_{da}+i\gamma_d,$$
$$R^{(1)}_2=c(k-k')-\frac{\hbar}{M}[-\mathbf{p}\cdot\mathbf{q}+q^2/2]-\omega_{ca}+i\eta, \quad (10)$$
$$R^{(1)}_3=c(k)-\frac{\hbar}{M}[\mathbf{p}\cdot\mathbf{k}+k^2/2]-\omega_{ba}+i\gamma_b.$$

Here $\hbar\omega_{ij}\equiv\hbar(\omega_i-\omega_j)$ is the energy difference between states i, and j, γ_i is the inverse lifetime of state i, and η is a vanishing positive quantity. Here and throughout, the process is understood to conserve photon momentum, but for clarity of presentation this is not explicitly indicated.

As described in the Appendix, intensity correlation functions for photon-photon scattering products contain a Fourier transform of the scattering amplitudes,

$$P(x_A,t_A,x_B,t_B)\propto\left|\int d\delta_{k'}V_{\mathbf{l}'\mathbf{k}'\mathbf{l}_0\mathbf{k}_0}\exp[ic\delta k'\tau_-]\right|^2, \quad (11)$$

where $\delta k'$ is the output photon energy shift, $x_{A,B}$ and $t_{A,B}$ are detection positions and times, respectively, and $\tau_-\equiv t_B-x_B/c-t_A+x_A/c$ is the difference in retarded times. This expression allows us to determine the time correlations for photon-photon scattering in a number of important cases.

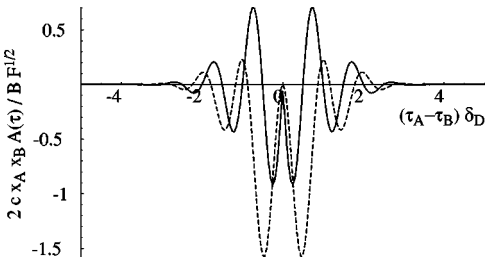

FIG. 2. Right-angle scattering amplitude vs time delay for the single-atom process of Fig. 1.

III. LARGE-ANGLE SCATTERING

The simplest configuration to understand is that of counterpropagating input beams producing counterpropagating output photons scattered at large angles. This is also the most convenient experimental geometry.

A. One-atom process

Scattering amplitudes and rates for right-angle scattering by the one-atom process are shown in Fig. 2 and Fig. 3, respectively. For the moment we ignore the statistical correction due to the $n_{a,\mathbf{p}}n_{c,\mathbf{p}-\mathbf{q}}$ term in Eq. (7), which will be considered separately. The vapor is treated as a gas of two-level atoms. The parameters are the Doppler width $\delta_D \equiv k(k_BT/M)^{1/2}$, where k_B is Boltzmann's constant, the radiative linewidth $\gamma_b = A_E/2$ where A_E is the Einstein A coefficient, and the detuning $\Delta \equiv ck - \omega_{ba}$, in the ratios $\gamma_b = 0.01\delta_D$, $\Delta = 2\pi\delta_D$. The amplitude and scattering rate are scaled by the accidental coincidence rate B, as described in Appendix A 2.

At this point it is important to note that the duration of the correlation signal is much shorter than the coherence lifetime of an individual atom, approximately γ_b^{-1}. In fact, the duration of the correlation signal is determined by the momentum distribution, a property of the medium as a whole. This can be explained in terms of the coherent summation of amplitudes for scattering processes occurring at different atoms. The process is coherent only when it is not possible, even in principle, to tell which atom participated. This clearly requires momentum conservation among the photons, but it also limits the duration of the atomic involvement. An atom acting as intermediary to transfer momentum $\mathbf{q}$ is displaced during the time it remains in the state c of Fig. 1. If this

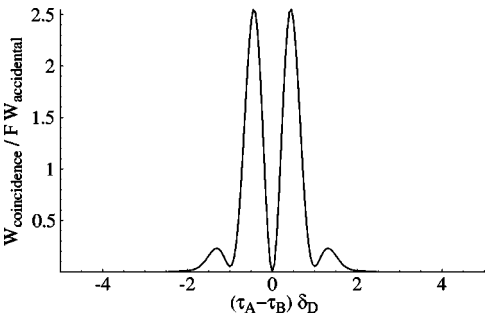

FIG. 3. Right-angle scattering rate vs time delay for the single-atom process of Fig. 1.

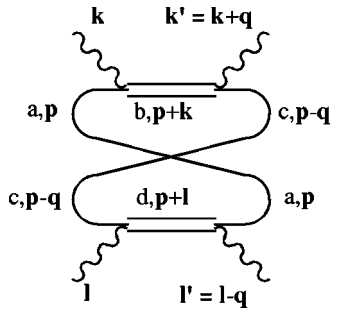

FIG. 4. Two-atom photon-photon scattering.

displacement is larger than the thermal deBroglie wavelength Λ, it becomes possible, in principle, to determine which atom participated. This limits the duration of the coherent process to $\delta\tau \sim \Lambda M/\hbar q$. The anticoincidence null at zero time difference reflects the fact that a single two-level atom, after emitting one photon, is guaranteed to be in an unexcited state, and thus incapable of immediately emitting a second photon [19,18]. The oscillations are essentially Rabi oscillations, damped by the progressive decoherence due to atomic motion and, to a lesser extent, the loss from spontaneous emission.

B. Simultaneous scattering

A second parametric process, simultaneous scattering, is described by the diagram of Fig. 4. The relevant terms in H'^4 contain

$$c^\dagger_{a,\mathbf{p}}c_{d,\mathbf{p}+\mathbf{l}'}a^\dagger_{\mathbf{l}'}c^\dagger_{c,\mathbf{p}-\mathbf{q}}c_{b,\mathbf{p}+\mathbf{k}}a^\dagger_{\mathbf{k}'}c^\dagger_{d,\mathbf{p}+\mathbf{l}'}c_{c,\mathbf{p}-\mathbf{q}}a_{\mathbf{l}}c^\dagger_{b,\mathbf{p}+\mathbf{k}}c_{a,\mathbf{p}}a_{\mathbf{k}} \tag{12}$$

or permutations $\mathbf{k}' \leftrightarrow \mathbf{l}'$, $\mathbf{k} \leftrightarrow \mathbf{l}$ for a total of four terms. Making the same assumption as before, this reduces to

$$n_{a,\mathbf{p}}n_{c,\mathbf{p}-\mathbf{q}}a^\dagger_{\mathbf{l}'}a^\dagger_{\mathbf{k}'}a_{\mathbf{l}}a_{\mathbf{k}}. \tag{13}$$

This process corresponds to the absorption of each photon by an atom before emission of either, and thus describes a two-atom process and is of the same order in the atomic number density as the Fermi and Bose corrections to single-atom scattering. The kinematic and geometric factors of Eq. (7) and Eq. (9) are the same for this process, and the resonance denominators are

$$R_1^{(2)} = c(k+l-k') - \frac{\hbar}{M}[\mathbf{p}\cdot\mathbf{l}' + l'^2/2] - \omega_{da} + i\gamma_d,$$

$$R_2^{(2)} = c(k+l) - \frac{\hbar}{M}[\mathbf{p}\cdot\mathbf{k} + k^2/2 + (\mathbf{p}-\mathbf{q})\cdot\mathbf{l} + l^2/2] - \omega_{ba} + i\gamma_b - \omega_{dc} + i\gamma_d, \tag{14}$$

$$R_3^{(2)} = c(k) - \frac{\hbar}{M}[\mathbf{p}\cdot\mathbf{k} + k^2/2] - \omega_{ba} + i\gamma_b.$$

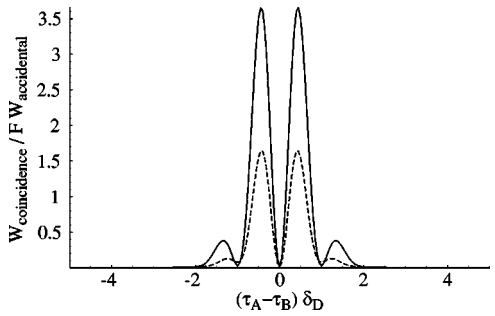

FIG. 5. Scattering rate vs time delay for Bose (solid) and Fermi (dashed) gases of phase-space density $\frac{1}{2}$.

C. Fermi and Bose gases

The statistical correction and two-atom scattering contributions add coherently to the one-atom scattering amplitude. This alters somewhat the form of the correlation signal. Notably, the signal no longer falls exactly to zero at zero time delay, due to the possibility of simultaneous scattering at two different atoms. Figure 5 shows scattering rates versus delay for Bose and Fermi gases with a phase-space density of one-half. Parameters are as for Fig. 2.

D. Ladder process

In atoms with a ''ladder'' level structure, in which three levels *a*-*c* are ordered in energy $\omega_c > \omega_b > \omega_a$ and connected by matrix elements $\mu_{ba}, \mu_{cb} \neq 0$, $\mu_{ca} = 0$, an additional process described by the diagram of Fig. 6 is possible. The relevant terms in H'^4 contain

$$c^\dagger_{a,\mathbf{p}} c_{d,\mathbf{p}+\mathbf{l}'} a^\dagger_{\mathbf{l}'} c^\dagger_{d,\mathbf{p}+\mathbf{l}'} c_{c,\mathbf{p}+\mathbf{k}+\mathbf{l}} a^\dagger_{\mathbf{k}'} \times c^\dagger_{c,\mathbf{p}+\mathbf{k}+\mathbf{l}} c_{b,\mathbf{p}+\mathbf{k}} a_{\mathbf{l}} c^\dagger_{b,\mathbf{p}+\mathbf{k}} c_{a,\mathbf{p}} a_{\mathbf{k}} \tag{15}$$

or permutations $\mathbf{k}' \leftrightarrow \mathbf{l}'$, $\mathbf{k} \leftrightarrow \mathbf{l}$ for a total of four terms. Making the same assumption as before, this reduces to

$$n_{a,\mathbf{p}} a^\dagger_{\mathbf{l}'} a^\dagger_{\mathbf{k}'} a_{\mathbf{l}} a_{\mathbf{k}} . \tag{16}$$

This process corresponds to the absorption of both photons by an atom before emission of either, and thus describes a one-atom process which is of the same order in the atomic number density as one-atom scattering. The kinematic and geometric factors of Eq. (7) and Eq. (9) are the same for this process, and the resonance denominators are

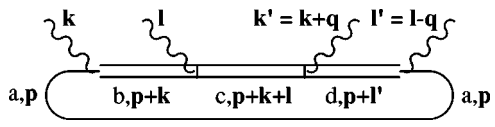

FIG. 6. ''Ladder'' process in a three-level atom.

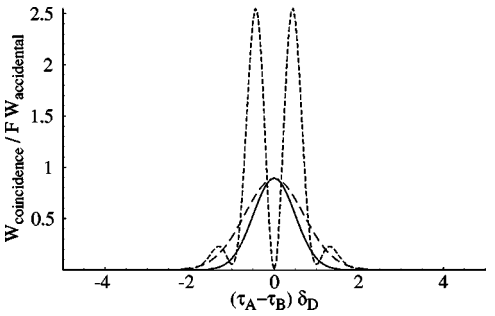

FIG. 7. Scattering rate vs time delay for the single-atom (short dashes), ladder (long dashes), and linear (solid) processes.

$$R_1^{(3)} = c(k+l-k') - \frac{\hbar}{M}[\mathbf{p}\cdot\mathbf{l}' + l'^2/2] - \omega_{da} + i\gamma_d ,$$

$$R_2^{(3)} = c(k+l) - \frac{\hbar}{M}[\mathbf{p}\cdot(\mathbf{k}+\mathbf{l}) + |\mathbf{k}+\mathbf{l}|^2/2] - \omega_{ca} + i\gamma_c , \tag{17}$$

$$R_3^{(3)} = c(k) - \frac{\hbar}{M}[\mathbf{p}\cdot\mathbf{k} + k^2/2] - \omega_{ba} + i\gamma_b .$$

E. Lorentz-model behavior

It is interesting to consider the case of a ladder atom with equal energy spacing $\omega_{cb} = \omega_{ba}$ and matrix elements $|\mu_{cb}|^2 = 2|\mu_{ba}|^2$. In this case the states *a*-*c* are equivalent to the lowest three levels of a harmonic oscillator, i.e., to a Lorentz model, and the medium is effectively linear for two-photon processes.

The amplitudes for the one-atom process of Eq. (4) and the ladder process of Eq. (15) partially cancel. The resulting signal is smaller and lacks oscillations, as shown in Fig. 7. Parameters are as for Fig. 2.

F. Background events

In addition to the photon-photon scattering processes, Rayleigh scattering (and Raman scattering for more complicated atoms) will create an uncorrelated coincidence background. This background is calculated in Appendix A. The coincidence signal, consisting of both the Lorentz-model atom photon-photon scattering signal and the incoherent background, is shown in Fig. 8. The peak coincidence rate

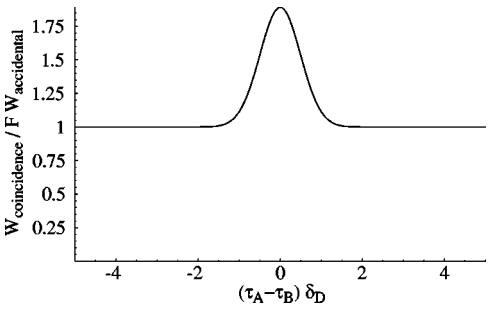

FIG. 8. Coincidence rate vs time delay for a Lorentz-model atomic medium. The constant background is accidental coincidences due to independent Rayleigh scattering events.

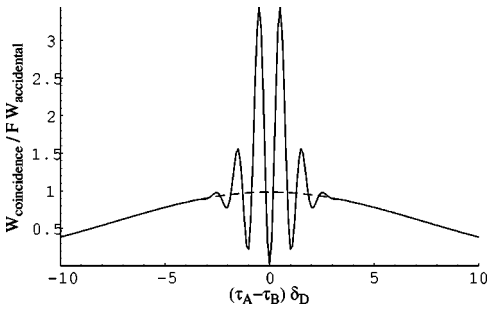

FIG. 9. Small-angle scattering rate vs time delay for nearly copropagating photons. The dashed curve shows the linear scattering signal.

(at $\delta\tau=0$) is nearly twice the background, accidental coincidence rate. In the limit of large detuning, it becomes exactly twice the accidental rate. This can be explained in analogy with the Hanbury-Brown-Twiss effect as follows: For the optimal geometry the drive beams are conjugates of each other $H(\mathbf{x})=G^*(\mathbf{x})$ and the detectors are in opposite directions. The linear atoms act to create a random index grating which scatters a chaotic but equal (up to phase conjugation) field to each detector. As expected for chaotic light [20], the fourth-order equal-time correlation function is twice the product of second-order correlation functions,

$$\langle E^2(\mathbf{x}_A,t)E^2(\mathbf{x}_B,t)\rangle=2\langle E^2(\mathbf{x}_A,t)\rangle\langle E^2(\mathbf{x}_B,t)\rangle. \quad (18)$$

IV. SMALL-ANGLE SCATTERING

Thus far the discussion has involved only large-angle scattering. In the context of cavity nonlinear optics all fields are propagating nearly along the optical axis of the cavity so it is necessary to consider scattering processes for nearly copropagating or nearly counterpropagating photons. As argued above, the temporal width of the correlation signal scales as $1/q$, the inverse of the momentum transfer. This is shown in Fig. 9 and Fig. 10, which show rates for scattering photons from beams in the x-z plane into the the y-z plane. In all cases the beam directions are 0.1 rad from the z axis. The coincidence distribution shows oscillations which die out on the time scale of the inverse Doppler width, and a nonoscillating pedestal with a width determined by the momentum transfer q.

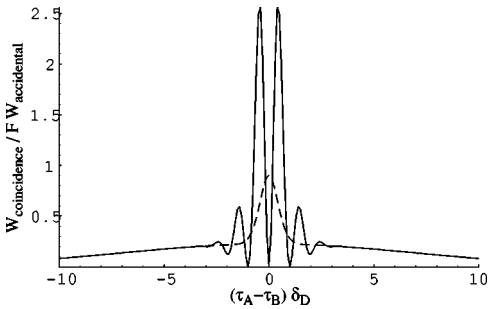

FIG. 10. Small-angle scattering rate vs time delay for nearly counterpropagating photons. The dashed curve shows the linear scattering signal.

The pedestal, however, does not correspond to the duration of the nonlinear process in this case. As above, by considering a ladder atom with the energy spacings and matrix elements of a harmonic oscillator we can isolate the linear optical behavior. This behavior includes the pedestal, but not the oscillations, indicating that the nonlinear optical process is still fast, with a time scale on the order of the inverse Doppler width.

V. LIMITATIONS ON SCATTERING ANGLE

Due to the limited width of the atomic momentum distribution, the resonance denominator $R_2^{(1)}$ is small if the input and output photons are not of nearly the same energy. Since the complete process must conserve photon momentum, input photons with net transverse momentum in the output photon direction will scatter less strongly. The width of this resonance is very narrow: a net transverse momentum $k_y+l_y\sim k\sqrt{k_BT/Mc^2}$ is sufficient that few atoms will be resonant. As $\sqrt{k_BT/Mc^2}$ is typically of order 10^{-6} in an atomic vapor, this would be a severe restriction on the transverse momentum content of the beams in a cavity nonlinear optics experiment. However, as shown in Fig. 10, the narrow resonance associated with $R_2^{(1)}$ contributes the linear response of the medium. The nonlinear response, which has the same resonance character as the ''ladder'' process, is not limited in this way because $R_2^{(3)}$ does not depend upon the output photon energies.

VI. OUTPUT POLARIZATION

The polarization of the output photons depends on the structure of the atom and can produce polarization-entangled photons. For example, if the input photons are propagating in the $\pm z$ directions and are x polarized, the two absorption events in the above diagram change the z component of angular momentum by $\delta m=\pm 1$. In order for the process to return the atom to its initial state, the two emission events must both produce $\delta m=\pm 1$ or both $\delta m=0$. For right-angle scattering with the detectors in the $\pm y$ directions, the output photons must therefore be either both x or both z polarized. If both polarizations are possible, the emitted photons are entangled in polarization, as well as in energy and in momentum.

VII. EXPERIMENT

Here we describe an experiment to directly measure the time duration of the photon-photon interaction in a transparent medium. In the scattering experiment, two off-resonance laser beams collide in a rubidium vapor cell and scattering products are detected at right angles. The process of phase-matched resonance fluorescence in this geometry has been described as spontaneous four-wave mixing [18], a description which applies to our off-resonant excitation as well. This geometry has been of interest in quantum optics for generating phase-conjugate reflection [21]. Elegant experiments with a barium atomic beam [19] showed antibunching

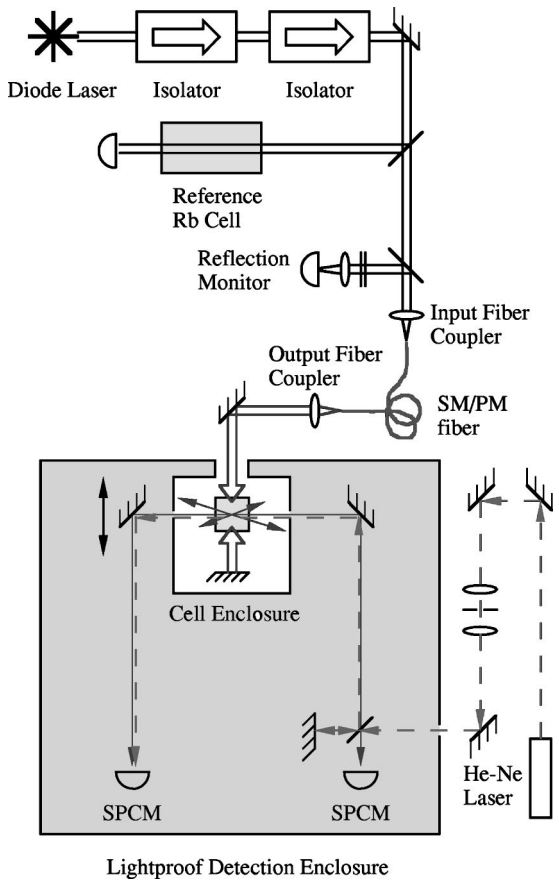

FIG. 11. Experiment schematic.

in multiatom resonance fluorescence, but a separation of time scales was not possible since the detuning, linewidth, and Doppler width were all of comparable magnitude.

A. Setup

The experimental setup is shown schematically in Fig. 11. A free-running 30 mW diode laser at 780 nm was temperature stabilized and actively locked to the point of minimum fluorescence between the hyperfine-split resonances of the D2 line of rubidium. Saturation spectroscopy features could be observed using this laser, indicating a linewidth $\delta\nu < 200$ MHz. This linewidth is small compared with the detuning from the nearest absorption line $\delta\nu = 1.3$ GHz. Direct observation of the laser output with a fast photodiode (3 dB rolloff at 9 GHz) showed no significant modulation in the frequency band 100 MHz–2 GHz. The laser beam was shaped by passage through a single-mode polarization-maintaining fiber, collimated and passed through a scattering cell to a retroreflection mirror. The beam within the cell was linearly polarized in the vertical direction. The beam waist (at the retroreflection mirror) was 0.026 cm$\times$0.023 cm (intensity FWHM, vertical $\times$ horizontal). The center of the cell was 1.9 cm from the retroreflection mirror, thus within a Rayleigh range of the waist. With optimal alignment, the laser could deliver 1.95 mW to the cell, giving a maximal Rabi frequency of $\Omega_{\mathrm{Rabi}} \approx 2\times10^9$ s^{-1}, significantly less than the minimal detuning of $\delta = 2\pi\times1.3$ GHz $= 8\times10^9$ s^{-1}. For this reason, we have neglected saturation of the transitions in the analysis.

The retroreflected beam returned through the fiber and was picked off by a beamsplitter. The single-mode fiber acted as a near-ideal spatial filter and the returned power through the fiber provides a quantitative measure of the mode fidelity on passing through the rubidium cell. With optimal alignment it was possible to achieve a mode fidelity (described below) of 36%.

The cell, an evacuated cuvette filled with natural abundance rubidium vapor, was maintained at a temperature of 330 K to produce a density of about 1.6×10^{10} cm^{-3}. Irises near the cell limited the field of view of the detectors. Stray light reaching the detectors was negligible, as were the detectors' dark count rates of <100 cps.

With the aide of an auxiliary laser beam, two single-photon counting modules (SPCMs) were positioned to detect photons leaving the detection region in opposite directions. In particular, photons scattered at right angles to the incident beams and in the direction perpendicular to the drive beam polarization were observed. Each detector had a 500 μm diameter active area and a quantum efficiency of about 70%. The detectors were at a distance of 70 cm from the center of the cell. The effective position of one detector could be scanned in two dimensions by displacing the alignment mirrors with inchworm motors. A time-to-amplitude converter and multichannel analyzer were used to record the time-delay spectrum. The system time response was measured using subpicosecond pulses at 850 nm as an impulse source. The response was well described by a Lorentzian of width 810 ps (FWHM).

Optimal alignment of the laser beam to the input fiber coupler could not always be maintained against thermal drifts in the laboratory. This affected the power of the drive beams in the cell but not their alignment or beam shape. These were preserved by the mode filtering of the fiber. Since the shape of the correlation function depends on beam shape and laser tuning but not on beam power, this reduction in drive power reduced the data rate but did not introduce errors into the correlation signal.

B. Experimental results

The time-delay spectrum of a data run of 45 h is shown in Fig. 12. The detectors were placed to collect back-to-back scattering products to maximize the photon-photon scattering signal. A Gaussian function $P(t_A - t_B)$ fitted to the data has a contrast $[P(0)-P(\infty)]/P(\infty)$ of 0.046 ± 0.008, a FWHM of 1.3 ± 0.3 ns, and a center of -0.07 ± 0.11 ns. This center position is consistent with zero, as one would expect by the symmetry of the scattering process. For comparison, a reference spectrum is shown. This was taken under the same conditions but with one detector intentonally misaligned by much more than the angular width of the scattering signal.

The angular dependence of the scattering signal was investigated by acquiring time-delay spectra as a function of detector position. To avoid drifts over the week-long acquisition, the detector was scanned in a raster pattern, remaining on each point for 300 s before shifting to the next. Points

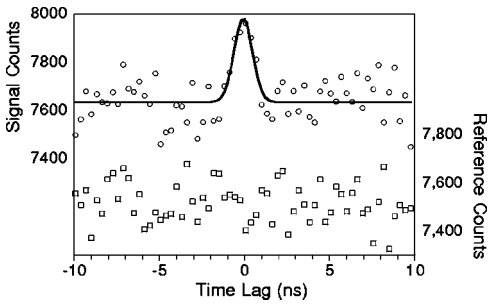

FIG. 12. Observed coincidence rates for right-angle photon-photon scattering. Circles show data acquired with detectors aligned to collect back-to-back scattering products. Squares show data acquired with detectors misaligned by 10 cm≈0.14 rad. The solid line is a Gaussian function fit to the data.

were spaced at 1 mm intervals. Total live acquisition time was 9 h per point. The aggregate time spectrum from each location was fitted to a Gaussian function with fixed width and center determined from the data of Fig. 12. The position-dependent contrast $C(x,y)$ is shown in Fig. 13. A negative value for the contrast means that the best fit had a coincidence dip rather than a coincidence peak at zero time. These negative values are not statistically significant. Fitted to a Gaussian function, $C(x,y)$ has a peak of 0.044 ± 0.010 and angular widths (FWHM) of 1.1 ± 0.7 mrad and 3.7 ± 0.4 mrad in the horizontal and vertical directions, respectively.

These angular widths are consistent with the expected coherence of scattering products [22]. Seen from the detector positions, the excitation beam is narrow in the vertical direction, with a Gaussian shape of beam waist $w_y=0.009$ cm, but is limited in the horizontal direction only by the apertures, of size $\Delta z=0.08$ cm. Thus we expect angular widths of 0.9 mrad and 3.25 mrad, where the first describes diffraction of a Gaussian, and the second describes diffraction from a hard aperture.

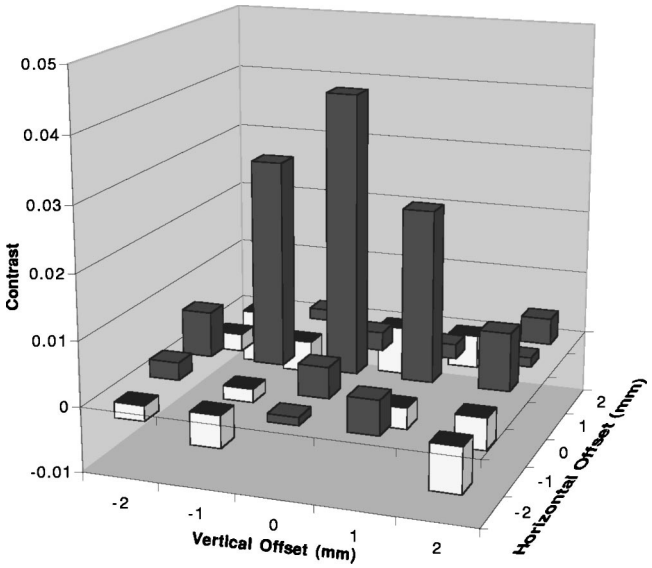

FIG. 13. Signal contrast vs detector displacement. A displacement of 1 mm corresponds to an angular deviation of 1.43 mrad.

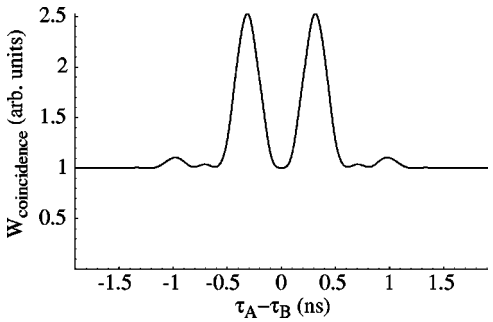

FIG. 14. Coincidence rates by photon-photon scattering theory: ideal case.

C. Comparison to theory

The photon-photon scattering theory presented above can be applied to the case of scattering in rubidium vapor. For scattering beams at 780 nm, we treat several lower levels ($F=1,2$ for Rb 87 and $F=2,3$ for Rb 85) and several upper levels ($F=0-3$ for Rb 87 and $F=1-4$ for Rb 85). The scattering process is always scattering at a single atom, as in Fig. 1. Other processes are too weak to have a considerable effect either due to the distance from resonance (ladder process) or the low degeneracy of the vapor (statistical correction and two-atom processes). The predicted scattering signal, including accidental coincidence background but before accounting for experimental imperfections, is shown in Fig. 14. The contrast is 1.53 and the FWHM is 870 ps. To compare to experiment, we account for the reduction of the signal due to experimental limitations. First, beam distortion in passing through the cell windows reduces the photon-photon scattering signal. Second, finite detector response time and finite detector size act to disperse the signal. None of these effects alters the incoherent scattering background.

Beam distortion is quantified by the fidelity factor,

$$F\equiv 4\frac{\left|\int d^3x\, G(\mathbf{x})H(\mathbf{x})\right|^2}{\left(\int d^3x[|G(\mathbf{x})|^2+|H(\mathbf{x})|^2]\right)^2}. \tag{19}$$

The greatest contrast occurs when H is the phase conjugate or time reverse of G, i.e., when $H(\mathbf{x})=G^*(\mathbf{x})$. In this situation $F=1$. Under the approximation that the field envelopes obey the paraxial wave equations

$$\frac{d}{dz}G=\frac{i}{2k}\nabla_\perp^2 G,$$
$$\frac{d}{dz}H=\frac{-i}{2k}\nabla_\perp^2 H, \tag{20}$$

Green's theorem can be used to show that the volume integral is proportional to the mode-overlap integral,

$$\int d^3x\, G(\mathbf{x})H(\mathbf{x})=\Delta z\int dx\, dy\, G(\mathbf{x})H(\mathbf{x}), \tag{21}$$

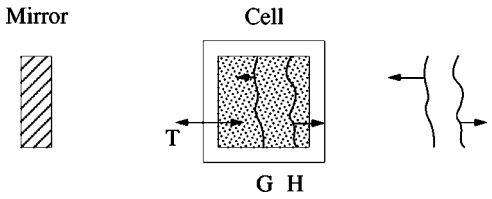

FIG. 15. Geometry for retroreflection measurements.

where the last integration is taken at any fixed z and Δz is the length of the interaction region. Similarly, the beam powers are invariant under propagation and the mode fidelity can be expressed entirely in terms of surface integrals as

$$F=4\left|\int dx\,dy\,G(\mathbf{x})H(\mathbf{x})\right|^2 \times\left[\int dx\,dy[|G(\mathbf{x})|^2+|H(\mathbf{x})|^2]\right]^{-2}. \tag{22}$$

The overlap of G and H also determines the efficiency of coupling back into the fiber, which allows us to determine F, as shown in Fig. 15. In terms of P_{in}, the power leaving the output fiber coupler, and P_{ret}, the power returned through the fiber after being retroreflected, this is

$$F=\frac{4}{(1+T^2)^2}\frac{P_{\mathrm{ret}}}{\eta T P_{\mathrm{in}}}, \tag{23}$$

where $\eta=0.883$ is the intensity transmission coefficient of the fiber and coupling lenses and $T=0.92$ is the transmission coefficient for a single pass through a cell window. We find $F=0.36\pm0.03$. The mode fidelity acts twice to reduce contrast, once as the drive beams enter the cell and again on the photons leaving the cell. This beam distortion has no effect on the incoherent scattering background, thus the visibility is reduced by F^2.

The finite time response of the detector system acts to disperse the coincidence signal over a larger time window. This reduces the maximum contrast by a factor of 0.27 and increases the temporal width to 1.62 ns. Similarly, the finite detector area reduces the maximum contrast by a factor of 0.81 and spreads the angular correlations by a small amount. The resulting predicted coincidence signal is shown in Fig. 16, along with the experimental points. Fitted to a Gaussian, the final signal contrast is 0.042 ± 0.007, where the uncertainty reflects the uncertainty in F. This is in good agreement with the observed contrast of 0.044 ± 0.010.

VIII. CONCLUSION

Time correlations in photon-photon scattering provide an indication of the time scale over which the atomic medium is involved in the interaction among photons in a nonlinear medium. It is found that the time scale is determined by the inhomogeneous broadening of the medium and the magnitude of the momentum transfer. For large-angle scattering, the time scale of involvement is $\delta\tau\sim\Lambda M/\hbar q$, while for small-angle scattering the time scale is $\delta\tau\sim\Lambda M/\hbar k$. As this time scale is shorter than the atomic relaxation time, calculations which contain an adiabatic elimination of the atomic degrees of freedom necessarily overlook the fastest dynamics in this process. We have measured the temporal and angular correlations in photon-photon scattering mediated by atomic rubidium vapor. We found good agreement between experiment and theory. The observed temporal correlations are of the order of one nanosecond, much faster than the system can relax by radiative processes. This is consistent with the prediction that the duration of the photon-photon interaction is determined by the inhomogeneous broadening of the vapor.

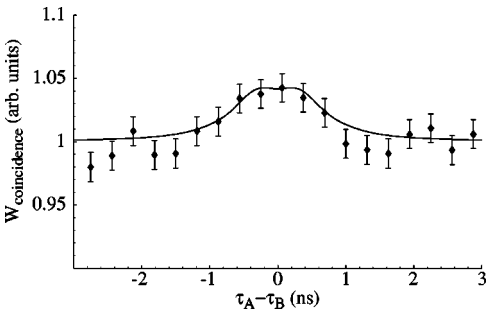

FIG. 16. Coincidence rates by photon-photon scattering theory: adjusted for beam shape, finite detection time, and detector area. Shown for comparison are the coincidence rate data taken at the phase-matching direction, scaled to the average background rate. Error bars indicate the statistical uncertainty.

APPENDIX A: PHOTON CORRELATIONS

1. Detection amplitudes

Unlike a genuine two-body collision process, atom-mediated photon-photon scattering has a preferred reference frame which is determined by the atomic momentum distribution. To calculate the photon correlations, we work in the ''laboratory'' frame and assume the momentum distribution is symmetric about zero. We consider scattering from two input beams with beam shapes $G(\mathbf{x})\equiv V^{-1/2}\Sigma_{\mathbf{k}}g(\mathbf{k})\exp[i\mathbf{k}\cdot\mathbf{x}]$ and $H(\mathbf{x})\equiv V^{-1/2}\Sigma_{\mathbf{l}}h(\mathbf{l})\exp[i\mathbf{l}\cdot\mathbf{x}]$, which are normalized as $\Sigma_{\mathbf{k}}|g(\mathbf{k})|^2=\Sigma_{\mathbf{l}}|h(\mathbf{l})|^2=1$. We further assume that the beams are derived from the same monochromatic source and are paraxial, i.e., that $g(\mathbf{k})$ is only appreciable in some small neighborhood of the average beam direction $\mathbf{k}_0$, and similarly for $h(\mathbf{l})$ around $\mathbf{l}_0$. The geometry is shown schematically in Fig. 17. For convenience, the

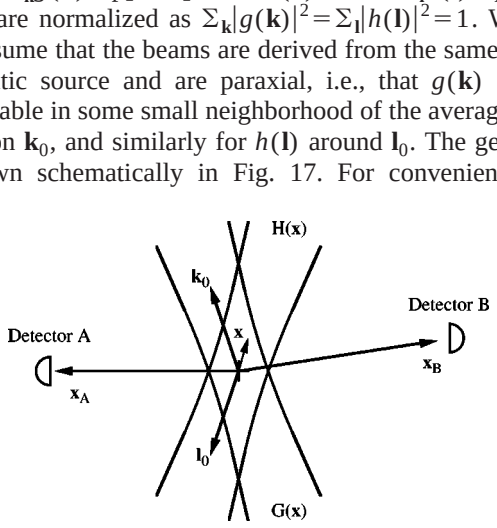

FIG. 17. Geometry of collision process.

beams are assumed to each contain one photon, so that the initial state of the field is

$$|\phi(0)\rangle = A_G^\dagger A_H^\dagger |0\rangle, \tag{A1}$$

where the creation operators $A_G^\dagger, A_H^\dagger$ are $A_G^\dagger \equiv \Sigma_{\mathbf{k}} g(\mathbf{k}) a_{\mathbf{k}}^\dagger$ and $A_H^\dagger \equiv \Sigma_{\mathbf{l}} h(\mathbf{l}) a_{\mathbf{l}}^\dagger$. Scaling of the result to multiple photons is obvious.

We use Glauber photodetection theory to determine the rates at which scattering products arrive at two detectors A and B at space-time points $(\mathbf{x}_A, t_A)$ and $(\mathbf{x}_B, t_B)$, respectively. We compute the correlation function in the Heisenberg representation,

$$P(\mathbf{x}_A, t_A, \mathbf{x}_B, t_B) = |\langle 0 | \Phi_H^{(+)}(\mathbf{x}_B, t_B) \Phi_H^{(+)}(\mathbf{x}_A, t_A) | \phi(0) \rangle_H|^2, \tag{A2}$$

where the photon field operator is

$$\Phi_H^{(+)}(\mathbf{x}, t) \equiv V^{-1/2} \sum_{\mathbf{k},\alpha} a_{\mathbf{k},\alpha}(t) \exp[i\mathbf{k}\cdot\mathbf{x}]. \tag{A3}$$

This field operator is similar to the positive frequency part of the electric field and is chosen so that $\Phi^{(-)}(\mathbf{x},t)\Phi^{(+)}(\mathbf{x},t)$ is Mandel's photon-density operator [23]. To make use of perturbation theory, Eq. (A2) is more conveniently expressed in the interaction representation as

$$\begin{aligned} P(\mathbf{x}_A, t_A, \mathbf{x}_B, t_B) &= |\langle 0 | \Phi_I^{(+)}(\mathbf{x}_B, t_B) U_I(t_B, t_A) \\ &\quad \times \Phi_I^{(+)}(\mathbf{x}_A, t_A) | \phi(t_A) \rangle_I|^2 \\ &= |\langle 0 | \Phi_I^{(+)}(\mathbf{x}_B, t_B) \Phi_I^{(+)}(\mathbf{x}_A, t_A) | \phi(t_A) \rangle_I|^2 \\ &\equiv |A(\mathbf{x}_A, t_A, \mathbf{x}_B, t_B)|^2, \end{aligned} \tag{A4}$$

where U_I is the interaction picture time-evolution operator, the interaction picture field operator is

$$\Phi_I^{(+)}(\mathbf{x}, t) = V^{-1/2} \sum_{\mathbf{k},\alpha} a_{\mathbf{k},\alpha} \exp[i(\mathbf{k}\cdot\mathbf{x} - ckt)], \tag{A5}$$

and in passing to the second line we have made the assumption that a detection at $(\mathbf{x}_A, t_A)$ does not physically influence the behavior of photons at $(\mathbf{x}_B, t_B)$ although there may be correlations.

The amplitude of joint detection is

$$\begin{aligned} A(\mathbf{x}_A, t_A, \mathbf{x}_B, t_B) &= \frac{(2\pi)^3}{V^2 \hbar} \sum_{\mathbf{k}'\mathbf{l}'} \exp[i(\mathbf{k}'\cdot\mathbf{x}_A - ck' t_A)] \\ &\quad \times \exp[i(\mathbf{l}'\cdot\mathbf{x}_B - cl' t_B)] \\ &\quad \times \sum_{\mathbf{kl}} g(\mathbf{k}) h(\mathbf{l}) V_{\mathbf{l}'\mathbf{k}'\mathbf{lk}} \\ &\quad \times \frac{1 - \exp[ic(k' + l' - k - l)t_A]}{c(k' + l' - k - l) + i\eta}. \end{aligned} \tag{A6}$$

Although $V_{\mathbf{l}'\mathbf{k}'\mathbf{lk}}$ depends strongly upon the magnitudes of the initial and final photon momenta through the resonance denominators of Eq. (10), it depends only weakly on their directions through the geometrical factors of Eq. (9). This and the assumption of paraxial input beams justify the approximation

$$\begin{aligned} \sum_{\mathbf{kl}} g(\mathbf{k}) h(\mathbf{l}) V_{\mathbf{l}'\mathbf{k}'\mathbf{lk}} &\approx V_{\mathbf{l}'\mathbf{k}'\mathbf{l}_0\mathbf{k}_0} \sum_{\mathbf{kl}} g(\mathbf{k}) h(\mathbf{l}) \delta_{\mathbf{k}+\mathbf{l},\mathbf{k}'+\mathbf{l}'} \\ &= V_{\mathbf{l}'\mathbf{k}'\mathbf{l}_0\mathbf{k}_0} \int d^3\mathbf{x}\, G(\mathbf{x}) H(\mathbf{x}) \\ &\quad \times \exp[-i(\mathbf{k}' + \mathbf{l}')\cdot\mathbf{x}]. \end{aligned} \tag{A7}$$

We can similarly treat the output photons in the paraxial approximation for the case that the detection points are far from the interaction region, i.e., that $x_A, x_B \gg x$. Making these approximations and dropping unphysical portions of the solution propagating inward from the detectors toward the source region, we find

$$\begin{aligned} A(\mathbf{x}_A, t_A, \mathbf{x}_B, t_B) &= \frac{-i}{\hbar c} \int k'\, d\, k'\, l' V_{\mathbf{l}'\mathbf{k}'\mathbf{l}_0\mathbf{k}_0} \\ &\quad \times \int d^3\mathbf{x} \frac{G(\mathbf{x}) H(\mathbf{x})}{|\mathbf{x}_A - \mathbf{x}||\mathbf{x}_B - \mathbf{x}|} \\ &\quad \times \exp\{i[\mathbf{k}'\cdot(\mathbf{x}_A - \mathbf{x}) - ck' t_A]\} \\ &\quad \times \exp\{i[\mathbf{l}'\cdot(\mathbf{x}_B - \mathbf{x}) - cl' t_B]\} \\ &\quad \times \theta(\tau_A)\theta(\tau_B), \end{aligned} \tag{A8}$$

where $c\tau_{A,B} \equiv ct_{A,B} - x_{A,B}$ are retarded times.

A final approximation ignores the slow variation of k', l' relative to that of the resonant $V_{\mathbf{l}'\mathbf{k}'\mathbf{l}_0\mathbf{k}_0}$. Further, we define $G'(\mathbf{x}) \equiv G(\mathbf{x}) \exp[ik_0\cdot\mathbf{x}]$, $H'(\mathbf{x}) \equiv H(\mathbf{x}) \exp[il_0\cdot\mathbf{x}]$, and $k' \equiv k_0' + \delta k'$, where $\mathbf{k}_0'$ is the value of $\mathbf{k}'$ which maximizes $V_{\mathbf{l}'\mathbf{k}'\mathbf{l}_0\mathbf{k}_0}$ subject to momentum and energy conservation. This gives a simple expression for the correlation function,

$$\begin{aligned} A(\mathbf{x}_A, t_A, \mathbf{x}_B, t_B) &= \frac{-ik' l'}{\hbar c} \exp[-ic(k_0'\tau_A + l_0'\tau_B)] \\ &\quad \times \int d\, \delta_{k'} V_{\mathbf{l}'\mathbf{k}'\mathbf{l}_0\mathbf{k}_0} \exp[ic\,\delta_{k'}(\tau_B - \tau_A)] \\ &\quad \times \int d^3\mathbf{x} \frac{G'(\mathbf{x}) H'(\mathbf{x})}{|\mathbf{x}_A - \mathbf{x}||\mathbf{x}_B - \mathbf{x}|} \\ &\quad \times \exp[i(\mathbf{k}_0 + \mathbf{l}_0 - \mathbf{k}_0' - \mathbf{l}_0')\cdot\mathbf{x}] \\ &\quad \times \theta(\tau_A)\theta(\tau_B). \end{aligned} \tag{A9}$$

This can be interpreted as consisting of a carrier wave, a Fourier transform of the scattering amplitude, and a coherent integration of the contributions from different parts of the interaction region. The spatial integral enforces phase matching in the photon-photon scattering process.

2. Detection rates

The probability for a coincidence detection at two detectors of specified area and in two specified time intervals is

$$P=\int d^2\mathbf{x}_A\, d^2\mathbf{x}_B c\, dt_A c\, dt_B |A(\mathbf{x}_A,t_A,\mathbf{x}_B,t_B)|^2, \tag{A10}$$

where the integral is over the detector surfaces (each assumed normal to the line from scattering region to detector) and over the relevant time intervals. This is more conveniently expressed in terms of a rate W of coincidence detections in terms of the detector solid angles $\delta\Omega_A$, $\delta\Omega_B$ and the difference in retarded arrival times $\tau_-\equiv\tau_B-\tau_A$,

$$W=c^2x_A^2x_B^2|A(\mathbf{x}_A,t_A,\mathbf{x}_B,t_B)|^2\delta\Omega_A\delta\Omega_B\, d\tau_-. \tag{A11}$$

Coincidence rate is largest when the detectors are placed in the directions which satisfy the phase-matching condition. We assume that $\mathbf{k}+\mathbf{l}=\mathbf{k}'+\mathbf{l}'=0$ and that the detectors are small compared to the source-detector distance, i.e., that $\delta\Omega_{A,B}\ll 1$. Under these conditions, the rate of coincidence events reduces to

$$W_{\text{scattering}}=\frac{k^4}{\hbar^2}\left|\int d\,\delta_{k'}V_{\mathbf{l}'\mathbf{k}'\mathbf{l}_0\mathbf{k}_0}\exp[ic\,\delta_{k'}\tau_-]\right|^2 \times\left|\int d^3x\, G(\mathbf{x})H(\mathbf{x})\right|^2\delta\Omega_B\delta\Omega_B\, d\tau_-. \tag{A12}$$

3. Signal contrast

In addition to the photon-photon scattering signal, uncorrelated Rayleigh and Raman scattering events give a background of accidental coincidences. The rate of scattering into a small solid angle $\delta\Omega$ is

$$W_{\text{BG}}=B\,\delta\Omega\int d^3x\, n_k, \tag{A13}$$

where

$$B\equiv\sum_{a,c}\int d^3\mathbf{p}\langle n_{a,\mathbf{p}}\rangle(1\pm\langle n_{c,\mathbf{p}'}\rangle)\frac{k_f^4c}{(2\pi)^3\hbar^2} \times\left|\sum_b\frac{(\mathbf{e}_f\cdot\boldsymbol{\mu}_{bc})^*\mathbf{e}_i\cdot\boldsymbol{\mu}_{ba}}{ck+\omega_{ab}-\frac{\hbar}{M}[\mathbf{p}\cdot\mathbf{k}+k^2/2]+i\gamma_b}\right|^2 \tag{A14}$$

and n_k is the number density of photons propagating in the $\mathbf{k}$ direction.

In terms of the beam-shape functions for two colliding beams, the rate of accidental coincidences is

$$W_{\text{accidental}}=B^2\left[\int d^3x|G(\mathbf{x})|^2+|H(\mathbf{x})|^2\right]^2\times\delta\Omega_A\delta\Omega_B\, d\tau_-. \tag{A15}$$

The ratio of coincidences due to photon-photon scattering to accidental background coincidences is thus

$$\frac{W_{\text{scattering}}}{W_{\text{accidental}}}=\frac{k^4}{4\hbar^2}\frac{F}{B^2}\left|\int d\,\delta_{k'}V_{\mathbf{l}'\mathbf{k}'\mathbf{l}_0\mathbf{k}_0}\exp[ic\,\delta_{k'}\tau_-]\right|^2, \tag{A16}$$

where F is the mode fidelity factor,

$$F\equiv 4\frac{\left(\int d^3x\, G(\mathbf{x})H(\mathbf{x})\right)^2}{\left(\int d^3x[|G(\mathbf{x})|^2+|H(\mathbf{x})|^2]\right)^2}. \tag{A17}$$

[1] J. Boyce and R. Chiao, Phys. Rev. A **59**, 3953 (1999).
[2] J. Boyce, J. Torres, and R. Chiao, Opt. Lett. **24**, 1850 (1999).
[3] J. Torres, J. Boyce, and R. Chiao, Phys. Rev. Lett. **83**, 4293 (1999).
[4] R. Y. Chiao, I. H. Deutsch, J. C. Garrison, and E. M. Wright, in *Frontiers in Nonlinear Optics, The Sergei Akhmanov Memorial Volume*, edited by H. Walther, N. Koroteev, and M. O. Scully (Institute of Physics Publishing, Bristol, 1992), pp. 151–182.
[5] I. Deutsch, R. Chiao, and J. Garrison, Phys. Rev. Lett. **69**, 3627 (1992).
[6] E. H. Lieb and W. Liniger, Phys. Rev. **130**, 1605 (1963).
[7] E. H. Lieb, Phys. Rev. **130**, 1616 (1963).
[8] P. Drummond and S. Carter, J. Opt. Soc. Am. B **4**, 1565 (1987).
[9] S. Carter, P. Drummond, M. Reid, and R. Shelby, Phys. Rev. Lett. **58**, 1841 (1987).
[10] P. Drummond and M. Hillery, Phys. Rev. A **59**, 691 (1999).
[11] M. Hillery and L. Mlodinow, Phys. Rev. A **30**, 1860 (1984).
[12] P. Drummond, Phys. Rev. A **42**, 6845 (1990).
[13] I. Abram and E. Cohen, Phys. Rev. A **44**, 500 (1991).
[14] M. O. Scully and W. E. Lamb, Jr., Phys. Rev. **159**, 208 (1967).
[15] M. Sargent III, D. Holm, and M. Zubairy, Phys. Rev. A **31**, 3112 (1985).
[16] P. Drummond and D. Walls, Phys. Rev. A **23**, 2563 (1981).
[17] W. H. Louisell, *Quantum Statistical Properties of Radiation*, Wiley Series in Pure and Applied Optics (John Wiley & Sons, New York, 1973).
[18] A. Heidmann and S. Reynaud, J. Mod. Opt. **34**, 923 (1987).
[19] P. Grangier *et al.*, Phys. Rev. Lett. **57**, 687 (1986).
[20] D. F. Walls and G. J. Milburn, *Quantum Optics* (Springer, Berlin, 1994).
[21] A. Gaeta and R. Boyd, Phys. Rev. Lett. **60**, 2618 (1988).
[22] T. Pittman, Y. Shih, D. Strekalov, and A. Sergienko, Phys. Rev. A **52**, R3429 (1995).
[23] L. Mandel and E. Wolf, *Optical Coherence and Quantum Optics* (Cambridge University Press, New York, 1995).